Research Square

Preprints are preliminary reports that have not undergone peer review.
They should not be considered conclusive, used to inform clinical practice,
or referenced by the media as validated information.

SIRT1 Restores Autophagic Flux to Attenuate Podocyte Injury in Experimental Membranous Nephropathy

Zhaocheng Dong
Beijing University of Chinese Medicine
Yunling Geng
Dongzhimen Hospital Affiliated to Beijing University of Chinese Medicine
Jingyi Tang
Dongzhimen Hospital Affiliated to Beijing University of Chinese Medicine
Zijing Cao
Dongzhimen Hospital Affiliated to Beijing University of Chinese Medicine
Wei Jing Liu
liuweijing-1977@hotmail.com
Dongzhimen Hospital Affiliated to Beijing University of Chinese Medicine
Baoli Liu
Beijing Hospital of Traditional Chinese Medicine

Research Article

Keywords: Membranous nephropathy, SIRT1, Passive Heymann Nephritis, Podocyte injury, Autophagic flux, C5b-9

Posted Date: August 15th, 2026

DOI: https://doi.org/10.21203/rs.3.rs-10613283/v1

License: This work is licensed under a Creative Commons Attribution 4.0 International License.
Read Full License

Additional Declarations: No competing interests reported.

Abstract

Background

Membranous nephropathy (MN), characterized by subepithelial immune deposits and podocyte injury, lacks targeted therapies addressing non-immunological injury mechanisms. SIRT1, a NAD^+-dependent deacetylase, regulates autophagy and cellular homeostasis, but its role in MN remains undefined.

Methods

We combined passive Heymann nephritis (PHN) rats and complement-injured podocytes to investigate SIRT1's function. Pharmacological activation (resveratrol/SRT1720) or $SIRT1^{\Delta Pod}$ models were employed. Assessments included proteinuria, histopathology, autophagic flux, and SIRT1 activity.

Results

SIRT1 activation in PHN rats reduced proteinuria and glomerular IgG and C5b-9 deposition, restored podocyte integrity and SIRT1 activity, resolved autophagic flux blockade. In podocytes, SIRT1 agonists attenuated complement-induced LDH release and cytoskeletal disruption, enhanced autophagosome-lysosome fusion. $SIRT1^{\Delta Pod}$ mice exhibited mild proteinuria without structural damage, implicating SIRT1 in functional maintenance.

Conclusion

SIRT1 protects podocytes in MN by restoring autophagic flux specifically through promoting autophagosome-lysosome fusion.

1. Introduction

Membranous nephropathy (MN), a leading cause of adult nephrotic syndrome, is characterized by subepithelial immune deposits on glomerular basement membranes (GBM), triggering podocyte injury and proteinuria[1]. Approximately 70–80% of idiopathic MN cases involve autoantibodies against podocyte antigens such as M-type phospholipase A2 receptor (PLA2R) and THSD7A[2]. These antibodies activate complement-independent pathways, inducing cytoskeletal disorganization, oxidative stress, mitochondrial dysfunction, and apoptosis in podocytes[3, 4]. Critically, C5b-9 disrupts autophagic flux by impairing lysosomal acidification and autophagosome-lysosome fusion, leading to accumulated cellular damage[5, 6].

Sirtuin 1 (SIRT1), an NAD^+-dependent deacetylase, is a key regulator of cellular homeostasis in kidney diseases[7]. It mitigates diabetic proteinuria, oxidative stress, and fibrosis by deacetylating targets

including FOXO3, Beclin-1, and NF-κB[8, 9]. SIRT1 activation enhances autophagy initiation and flux—a process essential for podocyte survival—by deacetylating autophagy-related proteins like Beclin-1[10, 11]. However, its role in MN-related podocyte injury remains unexplored.

This study investigates whether SIRT1-mediated deacetylation protects podocytes in experimental MN by promoting autophagosome-lysosome fusion. We demonstrate that SIRT1 activation reduces proteinuria and podocyte loss via restoring autophagy-lysosomal coordination. Our findings reveal a novel therapeutic axis targeting SIRT1-autophagy signaling to ameliorate MN progression.

2. Materials and method

2.1. Animals

All animal procedures were approved by the Animal Ethics Committee of Dongzhimen Hospital, Beijing University of Chinese Medicineand were performed in accordance with the relevant guidelines and regulations. Rats were deeply anesthetized with an intraperitoneal injection of sodium pentobarbital (1%, 50 mg/kg). Under deep anesthesia, they were euthanized by exsanguination via the abdominal aorta, and approximately 5 mL/100 g of blood was collected for biochemical analyses. Death was confirmed by the absence of heartbeat and respiration. For mice, blood was collected from the retro-orbital sinus (approximately 100–150 μL per mouse, followed by euthanasia by cervical dislocation. Death was confirmed by the absence of heartbeat and respiration.

Rat Model: Male Sprague-Dawley (SD) rats (SPF grade, 180–220 g) were purchased from Beijing Vital River Laboratory Animal Technology Co., Ltd. (Beijing, China). Passive Heymann Nephritis (PHN) was induced by intravenous injection of sheep anti-rat Fx1A antiserum (Probetex, PTX-002S). Rats with 24-h urinary protein > 100 mg at Day 14 were considered successfully modeled.

Genetic Mouse Model: Podocyte-specific SIRT1 knockout mice (female, 20 weeks) were generated on a C57BL/6J background by crossing $SIRT1^{flox/flox}$ mice with Nphs1-iCre transgenic lines, which were obtained from Jiangsu Jicui Yaokang Biotechnology Co., Ltd. (Jiangsu, China).

All animal procedures were approved by the Animal Ethics Committee of Dongzhimen Hospital, Beijing University of Chinese Medicine. All methods were performed in accordance with the relevant guidelines and regulations.

2.2. Experimental Groups

PHN Rats: Control, PHN Model, FK506 (1 mg/kg/day, oral gavage; GlpBio, GC16233), Resveratrol (RSV, 10 mg/kg/day, i.p.; Selleck, S1396). SIRT1 Mice: $SIRT1^{\triangle Pod}$ group (Nphs1-iCre-$SIRT1^{flox/flox}$), Control group($SIRT1^{flox/flox}$ littermates) .

2.3. Cell Culture

Podocytes: Immortalized mouse glomerular podocytes (MPC-5) were kindly provided by Professor Baoli Liu (Beijing Hospital of Traditional Chinese Medicine, Beijing, China). Cells were cultured in RPMI-1640 medium supplemented with 10% FBS and 10 U/mL IFN-γ at 33°C (proliferation), then differentiated at 37°C for 5–7 days. Complement Injury Model: Podocytes were stimulated with zymosan-activated serum (ZAS; 10%) for 2 h. ZAS was generated by incubating 1% zymosan (Sigma, Z4250) with serum (37°C, 1 h), followed by centrifugation (14,000 × g, 5 min) and filtration (0.8 μm).

2.4. Pharmacological Treatments

In Vivo: RSV was dissolved in 5% DMSO + 40% PEG300 + 5% Tween 80 + 50% H_2O. In Vitro: Podocytes were pretreated with RSV (10 μM) or SRT1720 (2.5 μM; GlpBio, GC17101) for 24 h before ZAS exposure.

2.5. Biochemical and Physiological Analyses

Urinary Protein: 24-h urinary protein quantified using Coomassie Brilliant Blue (CBB) assay (Nanjing Jiancheng, C035-2-1). Blood Biochemistry: Serum albumin, creatinine, urea nitrogen, and lipids measured using commercial kits (Nanjing Jiancheng). LDH Release: Podocyte damage assessed via CytoTox 96® assay (Promega, G1780).

2.6. Histopathology and Imaging

Light Microscopy: Kidney sections (3 μm) were stained with H&E, PAS, and PASM (Solarbio kits). Immunofluorescence: Frozen sections (5 μm) or podocytes were stained with antibodies against C3 (Abcam, ab200999), C5b-9 (Santa Cruz, sc-66190), Rat IgG (Abcam, ab150157), Nephrin (Abcam, ab216341), Podocin (Sigma, P0372), SIRT1 (Sigma, 07-131), LC3B (Abcam, ab192890), and LAMP1 (Santa Cruz, sc-20011). Nuclei were counterstained with DAPI. Electron Microscopy: Renal cortices fixed in glutaraldehyde (2.5%) and imaged using transmission electron microscopy (Hitachi H7650). Colocalization was quantified using confocal microscopy (Leica TCS SP5 II)

2.7. Western Blotting

Proteins extracted from renal cortices or podocytes using RIPA lysis buffer were separated by SDS-PAGE, transferred to PVDF membranes, and probed with antibodies against: Podocyte markers: Nephrin, Podocin, Synaptopodin (Abcam, ab259976). Autophagy markers: ATG5 (Proteintech, 10181-2-AP), ATG7 (Proteintech, 10088-2-AP), Beclin-1 (Abcam, ab210498), p62 (PM045, BioMol), LC3B (Abcam, ab192890). SIRT1 (Sigma, 07-131). GAPDH (Proteintech, 60004-1-Ig) served as the loading control.

2.8. SIRT1 Activity Assay

SIRT1 activity was measured in renal tissues or podocytes using a fluorometric kit (Abcam, ab156065) at excitation/emission wavelengths of 350/460 nm.

2.9. Statistical Analysis

Data are expressed as mean ± SD. Comparisons used one-way ANOVA with Tukey's post hoc test or unpaired t-tests (GraphPad Prism 9). Significance was set at $P < 0.05$.

3. Result

3.1 SIRT1 Activation Reduces Proteinuria and Protects Kidneys in PHN Rats

Passive Heymann nephritis (PHN) models were established as depicted in Fig. 1A. From day 0 to day 40 post-modeling, the 24-hour total urinary protein excretion in the model, FK506-treated, and RSV-treated groups was significantly higher than in the blank control group. However, urinary protein levels in the FK506 and RSV groups showed no significant difference compared to the model group during this period. By day 50, urinary protein excretion remained significantly elevated in the model, FK506, and RSV groups compared to the blank control group, but the RSV group exhibited a significant reduction in urinary protein compared to the model group (Fig. 1B). This demonstrates that SIRT1 activation effectively reduces urinary protein excretion. To rigorously demonstrate the therapeutic efficacy of SIRT1 activation in PHN rats, tissue collection ideally should have commenced after the RSV group showed significantly lower proteinuria than the model group on two consecutive measurements. However, given the known spontaneous remission of the PHN model and our preliminary data indicating scarce complement deposition in glomeruli of model rats sacrificed at day 60 post-modeling, tissue collection was initiated immediately upon the first statistically significant difference in proteinuria between the RSV and model groups (day 50). Blood samples were collected on day 50 for analysis of nephrotic syndrome-related and renal function parameters.

As shown in Fig. 1C, serum albumin was significantly lower in the model group than in the blank control group. Total cholesterol and triglycerides were significantly higher in the model group than in the blank control group. Compared to the blank control group, both the FK506 and RSV groups showed significantly elevated total cholesterol, but no significant difference in serum albumin or triglycerides. Serum albumin concentration was significantly higher in both the FK506 and RSV groups compared to the model group. Serum creatinine showed no significant difference among any groups compared to the blank control group. These results indicate that SIRT1 activation elevates serum albumin and lowers total cholesterol and triglyceride levels in PHN rats, demonstrating renal protective effects.

As shown in Fig. 2A, Hematoxylin and Eosin (HE) staining revealed no significant differences among groups. Periodic Acid-Schiff (PAS) and Periodic Acid-Schiff Methenamine Silver (PASM) staining showed significantly thickened glomerular basement membranes (GBM) in the model group compared to the blank control group. Both FK506 and RSV treatment attenuated GBM thickening relative to the model group. Electron microscopy (EM) imaging revealed foot process effacement and significantly thickened GBM in the model group podocytes compared to controls, along with enlarged lysosomes within podocytes. Both FK506 and RSV treatment ameliorated foot process effacement and GBM thickening compared to the model group. Notably, podocytes in the RSV group contained significantly more numerous and enlarged lysosomes than those in the model group. Immunofluorescence staining detected IgG, C3, and C5b-9 deposition in the glomeruli of the model group. Deposition of IgG, C3, and C5b-9 was reduced in both the FK506 and RSV groups compared to the model group. Glomerular SIRT1

fluorescence intensity in the blank control group was similar to that in tubules. In the model group, glomerular SIRT1 fluorescence was significantly weaker than tubular SIRT1. The disparity between glomerular and tubular SIRT1 fluorescence intensity observed in the model group was partially restored in the RSV group. However, glomerular SIRT1 fluorescence in the FK506 group remained significantly weaker than tubular SIRT1. Collectively, these findings demonstrate that SIRT1 activation effectively ameliorates renal pathological damage in PHN rats.

As shown in Fig. 2B, renal expression of the podocyte marker proteins Nephrin, Podocin, and Synaptopodin was significantly reduced in the model group compared to the blank control group. Nephrin expression was significantly higher in both the FK506 and RSV groups compared to the model group. Podocin expression showed an increasing trend in the FK506 and RSV groups relative to the model group, but the difference was not statistically significant. Synaptopodin expression in the RSV group showed no significant difference compared to the model group. Synaptopodin expression in the FK506 group was lower than in the model group, but this difference also did not reach statistical significance.

To confirm that the therapeutic effect on PHN and glomerular protection was mediated through SIRT1 activity, we measured renal SIRT1 activity across groups. As shown in Fig. 2C, renal SIRT1 activity was significantly lower in both the model group and the FK506 group compared to the blank control group. Renal SIRT1 activity in the RSV group was significantly higher than in the model group. This indicates that activating glomerular SIRT1 activity protects the kidneys in PHN rats. The expression of SIRT1 protein in each group of renal tissues is shown in Figure S1.

3.2 SIRT1 Activation Attenuates Complement Attack-Induced Podocyte Injury

Prior to drug intervention, the effects of different concentrations of SIRT1 activators (RSV, SRT1720) on podocytes were assessed. By measuring lactate dehydrogenase (LDH) release rate, the maximum non-toxic concentration was selected for subsequent interventions. The final concentrations used were 10 μM for RSV and 2.5 μM for SRT1720 (Figure S2). Podocytes were incubated with complement serum for 2 hours to model sublytic C5b-9 injury to glomerular visceral epithelial cells (podocytes) in membranous nephropathy patients. As shown in Fig. 3A, both the RSV-treated and SRT1720-treated groups significantly reduced the LDH release rate in the podocyte complement injury model. This indicates that both SIRT1 activators, RSV and SRT1720, attenuate complement-mediated podocyte injury.

As shown in Fig. 3B, podocyte SIRT1 activity was significantly lower in the model group than in the blank control group. SIRT1 activity in the RSV group was significantly higher than in the model group and showed no significant difference compared to the blank control group. SIRT1 activity in the SRT1720 group was significantly higher than in both the model group and the blank control group. These findings demonstrate that restoring podocyte SIRT1 activity confers protection against injury.

As shown in Fig. 3C, expression of the podocyte marker proteins Podocin and Synaptopodin was significantly reduced in the model group compared to the blank control group. Podocin expression in both the RSV and SRT1720 groups was significantly lower than in the blank control group, but significantly higher than in the model group. Synaptopodin expression was significantly higher in both the RSV and SRT1720 groups compared to the model group. Notably, Synaptopodin expression in the SRT1720 group showed no significant difference from the blank control group. SIRT1 expression was significantly lower in the model group than in the blank control group. Both RSV and SRT1720 treatment significantly increased SIRT1 expression compared to the model group, restoring it to levels comparable to the blank control group (no significant difference).

As shown in Fig. 3D, immunofluorescence staining revealed podocyte atrophy in the model group. Phalloidin-FITC staining showed disorganized cytoskeletal structure and reduced Podocin fluorescence intensity in the model group. Both RSV and SRT1720 treatment ameliorated cytoskeletal disorganization and increased Podocin fluorescence intensity compared to the model group. To confirm the podocyte-protective effect mediated by activating SIRT1 activity, SIRT1 expression and activity were measured in podocytes across groups. Immunofluorescence staining localized SIRT1 primarily to the nucleus. SIRT1 fluorescence intensity was reduced in the model group compared to the blank control group. Both RSV and SRT1720 treatment increased SIRT1 fluorescence intensity relative to the model group.

3.3 SIRT1 Regulates Autophagy in Renal Tissue and Podocytes

As shown in Fig. 4A, renal expression of ATG7, Beclin-1, and p62 was significantly elevated in the model group rats compared to the blank control group. LC3 levels showed a non-significant increasing trend in the model group, while ATG5 expression exhibited no significant difference compared to controls.

In the FK506-treated group, renal ATG5 expression was significantly lower than in the blank control group. Renal ATG7 expression was significantly lower than in the model group but showed no significant difference compared to the blank control group. Renal Beclin-1, p62, and LC3 levels showed no significant difference compared to the blank control group.

In the RSV-treated group, renal Beclin-1 expression was significantly lower than in both the blank control and model groups. Renal ATG7 expression was significantly lower than in the model group but showed no significant difference compared to the blank control group. Renal ATG5, p62, and LC3 levels showed no significant difference compared to the blank control group. These findings indicate that renal injury in PHN rats leads to increased autophagy levels. FK506 exerts its therapeutic effect primarily through immunomodulation, without significantly affecting the overall degree of renal autophagy.

However, whole-kidney Western blotting (WB) cannot accurately reflect autophagy levels specifically within glomerular podocytes. Therefore, we also performed immunofluorescence staining. As shown in Fig. 4B, glomerular ATG5 fluorescence intensity showed no significant difference between the model group and the blank control group. Both FK506 and RSV groups exhibited a slight decrease in glomerular

ATG5 fluorescence intensity compared to the blank control and model groups. Glomerular ATG7 fluorescence intensity was significantly higher in the model group than in the blank control group. Both FK506 and RSV groups showed glomerular ATG7 fluorescence intensity comparable to the blank control group (no significant difference). Glomerular Beclin-1 fluorescence intensity showed no significant differences among the blank control, model, FK506, and RSV groups. In summary, significant differences in glomerular ATG5, ATG7, or Beclin-1 fluorescence intensity were not observed across the groups.

As shown in Fig. 4C, renal p62 fluorescence intensity was higher in the model group than in the blank control group, while LC3 fluorescence intensity showed only a non-significant increase. Both FK506 and RSV groups exhibited lower renal p62 fluorescence intensity than the model group, with good colocalization between p62 and LC3. Renal p62 fluorescence intensity in the FK506 group was higher than in the RSV group. This suggests that SIRT1 activation suppresses autophagy accumulation as indicated by reduced p62 with restored LC3-p62 colocalization.

As shown in Fig. 5A, podocyte p62 expression was significantly elevated in the model group compared to the blank control group. ATG5, ATG7, Beclin-1, and LC3 levels showed increasing trends in the model group, but the differences were not statistically significant. In the RSV-treated group, podocyte ATG5 expression showed no significant difference compared to blank control or model groups. Podocyte ATG7 expression was significantly lower than in both blank control and model groups. Podocyte p62 expression was significantly higher than in the blank control group but significantly lower than in the model group. Podocyte Beclin-1 and LC3 levels showed no significant difference compared to blank control or model groups. In the SRT1720-treated group, podocyte ATG5 expression showed no significant difference compared to blank control or model groups. Podocyte ATG7 expression was significantly lower than in both blank control and model groups. Podocyte p62 expression was significantly lower than in the model group but showed no significant difference compared to the blank control group. Podocyte Beclin-1 and LC3 levels showed no significant difference compared to blank control or model groups.

As shown in Figs. 5B-E, podocyte fluorescence intensity for ATG5, ATG7, Beclin-1, and p62 was higher in the model group than in the blank control group. Podocyte LC3 fluorescence intensity showed no significant difference between model and blank control groups, but exhibited poor colocalization with p62. Both RSV and SRT1720 groups showed lower podocyte fluorescence intensity for ATG5, ATG7, Beclin-1, and p62 compared to the model group, along with improved LC3-p62 colocalization.

3.4 SIRT1 Promotes Autophagosome-Lysosome Fusion

As shown in Fig. 6A, colocalization of LC3 and LAMP1 in the glomeruli of the model group rats was significantly reduced compared to the blank control group. The RSV-treated group showed improved LC3-LAMP1 colocalization in the glomeruli relative to the model group. The FK506-treated group exhibited a modest improvement in glomerular LC3-LAMP1 colocalization compared to the model group.

As shown in Figs. 6B-D, podocytes in the model group displayed significantly reduced colocalization of LAMP1 with ubiquitin (Ub), LC3 with LAMP1, and Cortactin (CTTN) with LAMP1 compared to the blank control group. Both the RSV-treated group and the SRT1720-treated group demonstrated improved colocalization of LC3-Ub, LC3-LAMP1, and CTTN-LAMP1 in podocytes relative to the model group.

3.5 SIRT1 Regulates Autophagic Flux Through Deacetylation

Deacetylation is a key mechanism by which SIRT1 exerts its effects. We further investigated the deacetylation function of SIRT1. As shown in Figs. 7A-B, co-immunoprecipitation assays demonstrated an interaction between SIRT1 and both ATG7 and Beclin-1 in the renal tissues of rats and in mouse podocytes across the experimental groups. Furthermore, Figs. 7C-D show that co-immunoprecipitation revealed an interaction between SIRT1 and CTTN in the renal tissues of rats and mouse podocytes. The above results indicate that SIRT1 interacts with the key autophagy proteins ATG7 and Beclin-1, as well as the fusion protein CTTN. This suggests that the protective effects of SIRT1 activation in both the rat PHN model and the podocyte complement injury model are likely achieved by deacetylating these target proteins, thereby promoting autophagosome-lysosome fusion.

3.6 Renal Injury in Aged SIRT1$^{\triangle Pod}$ Mice

As shown in Fig. 8A, podocyte-specific SIRT1 muted mice exhibited significantly higher urinary albumin-to-creatinine ratio (UACR) and total cholesterol levels compared to their littermate negative control mice. However, no significant differences were observed in serum albumin, serum creatinine, or triglycerides between the knockout mice and their littermate controls.

As shown in Fig. 8B, Hematoxylin and Eosin (HE) staining revealed no significant differences in glomerular morphology between the littermate negative control mice and the SIRT1$^{\triangle Pod}$ mice. Periodic Acid-Schiff (PAS) staining also showed no significant changes in the glomeruli of SIRT1$^{\triangle Pod}$ mice compared to controls. Immunofluorescence staining detected no deposition of IgG or complement C3 in either group.

As shown in Fig. 8C, the expression levels of the podocyte marker proteins Nephrin and Podocin in the kidneys of SIRT1$^{\triangle Pod}$ mice showed no significant difference compared to the littermate negative controls.

These findings indicate that although the loss of SIRT1 specifically in podocytes did not cause overt structural damage or an inflammatory response in this aged model, it led to podocyte dysfunction, as evidenced by the increased proteinuria and hypercholesterolemia.

4. Discussion

This study establishes that SIRT1-mediated deacetylation protects podocytes in membranous nephropathy (MN) by restoring autophagic flux through promoting autophagosome-lysosome fusion. Using rat PHN and podocyte complement injury models, we demonstrate that pharmacological SIRT1 activation significantly reduces proteinuria and glomerular pathology, directly mitigates complement-mediated podocyte injury independent of immunosuppression and rescues autophagic flux by enhancing lysosomal fusion. These findings position SIRT1 as a key therapeutic target to protect against podocyte injury to alleviate MN.

Our study provides compelling evidence for a novel, non-immunosuppressive, cytoprotective role of SIRT1 in the pathogenesis of MN. Using a combination of the classic passive Heymann nephritis (PHN) rat model, which faithfully recapitulates key features of human MN [12, 13]. We demonstrated that the SIRT1 activator RSV significantly reduced 24-hour urinary protein excretion, elevated serum albumin levels, and ameliorated lipid metabolism disorders in PHN rats. Histological analysis revealed that the RSV-treated group exhibited attenuated glomerular basement membrane thickening, reduced foot process effacement, and decreased deposition of IgG, C3, and C5b-9. These findings are highly consistent with existing research. Notably, while FK506 reduced immune deposition, it showed no significant regulatory effect on SIRT1 activity or podocyte marker protein expression, suggesting that the protective mechanism of SIRT1 is independent of classical immunosuppressive pathways.

A key pathological feature of podocyte injury in MN is damage induced by sublytic doses of C5b-9 deposition. Among the three complement activation pathways, the classical pathway is triggered by antigen-antibody complexes, the alternative pathway is activated by microbial particles, and the lectin pathway relies on pathogen-associated carbohydrate structures. IgG4 antibodies deposited in the glomeruli of MN patients predominantly activate complement via the lectin and alternative pathways, forming sublytic membrane attack complexes (MAC) [14, 15]. This sublytic MAC does not directly lyse cells but inserts into the podocyte membrane, activating intracellular signaling pathways, leading to podocyte injury and proteinuria [1]. In addition to MAC, the C3a/C3aR inflammatory pathway has also been implicated in MN podocyte injury [16, 17]. This study employed zymosan-activated serum (simulating non-classical pathways) to directly generate MAC for stimulating podocytes, aiming to focus on the core injurious role of MAC. A central discovery of our research is the elucidation of how SIRT1 protects podocytes. Our data indicate that in response to complement-mediated injury, podocytes initiate an autophagic response, evidenced by the accumulation of autophagosomes. However, this response is ultimately maladaptive due to a downstream blockade in the autophagic pathway, leading to a pathological buildup of autophagic vesicles—a state of "autophagic constipation" or impaired flux. This phenomenon of blocked autophagic flux contributing to cellular injury is a recognized feature of complement-attacked podocytes [5]. Our results compellingly show that SIRT1 activation resolves this critical blockade.

While the role of SIRT1 as an NAD^+-dependent deacetylase in promoting autophagy is well-established the specific mechanisms can be multifaceted [8, 18–20]. Many studies have focused on SIRT1's ability to deacetylate transcription factors like FoxO, which in turn upregulate genes such as Rab7 to facilitate

autophagosome-lysosome fusion [21–23]. However, our research points towards a more direct, potentially FoxO- and Rab-independent, mechanism of action at the level of the core autophagic and fusion machinery.

It is noteworthy that current research on SIRT1 regulation of complement-mediated podocyte injury is extremely limited: Liu et al. reported that crocin upregulated SIRT1 in Heymann nephritis rats, but the model exhibited abnormally low urinary protein levels, limiting the reference value of their conclusion. Studies in other fields (e.g., alcoholic liver injury, ischemia-reperfusion injury) merely suggested an association between SIRT1 and the complement system without elucidating its cytoprotective mechanism [24, 25]. Therefore, this study is the first to reveal that SIRT1 activators (RSV/SRT1720) significantly mitigate complement MAC-mediated podocyte injury (manifested as reduced LDH release and restored cytoskeletal protein expression), filling the knowledge gap in the "SIRT1-complement-podocyte" regulatory axis and providing a novel rationale for targeted therapy in MN.

This study reveals that SIRT1 activation can stimulate autophagy, restore autophagic flux, promote autophagosome-lysosome fusion, and thereby exert protective effects on podocytes. We found that in the PHN model group, renal expression of ATG7, Beclin-1, and p62 was significantly elevated. However, immunofluorescence revealed an accumulation of autophagosomes alongside decreased expression of the lysosomal marker LAMP1 in glomerular podocytes, indicating the presence of autophagic flux blockade. This phenomenon aligns with C5b-9-mediated impairment of autophagosome-lysosome fusion observed in podocytes of MN patients. Following SIRT1 intervention, the number of autophagosomes in podocytes decreased, while lysosomal numbers increased, and autophagosome-lysosome fusion was restored. This confirms that SIRT1 activation rescues the integrity of autophagic flux. Numerous studies indicate that SIRT1 effectively regulates autophagy [11]. SIRT1 is known to form direct protein complexes with and deacetylate essential components of the autophagic machinery, including ATG5, ATG7, and LC3 [26–28]. During the initiation phase of autophagy, the BECN1-PIK3C3 complex is one of the key proteins for autophagosome formation. SIRT1 activates this complex and initiates autophagy by deacetylating these components [10]. Subsequently, LC3 (bound to the autophagosome surface), the E1-like enzyme ATG7, and ATG5 (within the E3-like enzyme ATG12-ATG5-ATG16L1 complex) can all be activated by SIRT1-mediated deacetylation [18]. SIRT1-mediated deacetylation of ATG5 and ATG7 has a well-defined biological function, namely enhancing autophagic activity [11]. These two proteins are indispensable components in the process of autophagosome elongation and formation, and the enhancement of their activity directly leads to an increase in autophagic flux, facilitating the clearance of damaged organelles. Numerous studies have reported the deacetylation of Beclin-1 by SIRT1 [18, 29]. SIRT1 directly interacts with Beclin-1 and specifically deacetylates its two lysine residues, K430 and K437, thereby activating the Beclin-1-dependent autophagy pathway [10, 29–31]. Our research results show that in the rat PHN model and the podocyte injury model, activating SIRT1 can reduce ATG7 and Beclin-1. This seems to be contrary to the current mainstream result. Therefore, we further conducted research on the fusion of autophagosomes and lysosomes.

CTTN is a potent promoter of autophagosome-lysosome fusion, and its activation, as well as the achievement of fusion function, also relies on deacetylation [32]. Many studies indicate that SIRT1 can deacetylate CTTN, and this deacetylation is a critical step in promoting cell migration [33–35]. Iwahara et al. using an inactive mutant of SIRT1 (H355Y) demonstrated that the deacetylase activity of SIRT1 is essential for the normal function of CTTN, and the repeat domain of the CTTN protein is a key region targeted by SIRT1 for deacetylation [35]. Acetylation of this region (mediated by p300) reduces the binding affinity of CTTN to F-actin, thereby inhibiting cell migration. SIRT1, by deacetylating this region, restores or enhances the binding of CTTN to actin, thus promoting cell movement and invasion [34, 35]. Therefore, SIRT1 can also promote the fusion of autophagosomes with lysosomes by deacetylating CTTN [11]. Therefore, SIRT1 protects podocytes directly by regulating autophagy and preserving autophagic flux through deacetylation.

A rigorous discussion requires a critical appraisal of the tools employed. We utilized resveratrol and SRT1720 as pharmacological activators of SIRT1. While widely used, the specificity of these compounds has been a subject of intense debate. Multiple studies using native, non-fluorophore-tagged substrates have shown that these molecules do not directly activate SIRT1 in vitro and that previously reported activation was likely an artifact of the fluorophore used in the assay kits [36]. Furthermore, these compounds are known to be promiscuous, with numerous off-target effects[36]. While our genetic model ($SIRT1^{\Delta Pod}$) supports a SIRT1-dependent mechanism, future pharmacological studies should employ more specific and physiologically relevant methods of SIRT1 activation. A superior strategy is the use of NAD^+ precursors, such as nicotinamide mononucleotide (NMN) or nicotinamide riboside (NR). These compounds boost the cellular pool of the essential SIRT1 co-substrate, NAD^+, thereby enhancing the activity of SIRT1 and other sirtuins in a more natural, dose-dependent manner [37, 38]. Studies have already shown that NMN can enhance SIRT1 expression and rescue podocyte injury in other models of kidney disease lending strong support to this approach [39, 40]. Future experiments should validate our key findings using NMN and employ non-fluorophore-based biochemical assays, such as HPLC or mass spectrometry, to measure the deacetylation of native SIRT1 substrates in podocytes [41–43].

The primary limitation of our study is its preclinical nature. While the PHN model is robust, the ultimate validation of our findings must come from human studies [12, 13]. Currently, there is a significant lack of data on the status of the SIRT1-autophagy axis in human MN. Extensive searches revealed no published proteomic, transcriptomic, or immunohistochemical studies that have systematically quantified SIRT1, LC3B, and p62 in human MN biopsy samples. Therefore, a critical next step is to analyze human kidney biopsy repositories. Using proteomics on archived biopsy tissues is feasible and would be invaluable for correlating SIRT1 expression levels and autophagy markers (like LC3B/p62 ratio) with disease severity and patient outcomes [44, 45].

Furthermore, although tissue collection was performed early in this study (at day 60) to circumvent the spontaneous remission phase of the PHN model, this may have led to an underestimation of RSV's long-term efficacy. The cell-specific mechanism requires further elucidation; specifically, podocyte-specific SIRT1 knockout mice are needed to clarify its cell-autonomous role in autophagy regulation. Finally, any

basic research must ultimately translate to clinical applications. Future studies could involve anti-PLA2R antibody monitoring to evaluate the clinical value of SIRT1 activators in treating MN.

5. Conclusion

In conclusion, our study demonstrates that SIRT1 activation confers a protective effect against podocyte injury in experimental membranous nephropathy, primarily by restoring autophagic flux through the promotion of autophagosome-lysosome fusion. Contrary to the simplistic paradigm of SIRT1 as a universal autophagy inducer, our findings reveal a more nuanced mechanism: sublytic C5b-9 attack triggers a compensatory but pathologically blockaded autophagic response, characterized by the accumulation of autophagic substrates. SIRT1 does not globally suppress this response; instead, it reprograms the dysfunctional autophagic process by specifically rectifying the fusion defect. This is achieved through the deacetylation of key regulators like CTTN, which enhances the efficiency of the final fusion step. Consequently, the restoration of autophagic flux normalizes the entire process, leading to the clearance of damaged proteins and organelles and ultimately attenuating podocyte injury and proteinuria. Our work positions SIRT1 not as a mere on/off switch for autophagy, but as a critical modulator of autophagic quality and flow, offering a novel and promising non-immunosuppressive therapeutic strategy for MN.

Declarations

Competing interests

The authors declare that they have no competing interests.

Funding

This work was supported by the National Key Research and Development Program of China (No. 2023YFC3503501 & 2023YFC3503504), the Fundamental Research Funds for the Central Universities (No. 2025-JYB-XJSJJ005) and the Horizontal Project (HX-DZM-202325). The authors declare no conflicts of interest.

Availability of data and materials

The datasets used and/or analysed during the current study are available from the corresponding author on reasonable request.

Author Contribution

This study was conceived and designed by W.J. Liu and B. Liu; experiments were performed by Z. Dong, Y. Geng, Z. Cao, J. Tang; Y. Geng provided advice and materials; and Z. Dong wrote the manuscript with input from all authors.

Data Availability

The datasets used and/or analysed during the current study are available from the corresponding author on reasonable request.

References

1. Couser WG (2017) Primary Membranous Nephropathy. Clin J Am Soc Nephrol 12(6):983–997
2. Sethi S, Fervenza FC (2024) Membranous nephropathy-diagnosis and identification of target antigens. Nephrol Dial Transpl 39(4):600–606
3. Kistler AD, Salant DJ (2024) Complement activation and effector pathways in membranous nephropathy. Kidney Int 105(3):473–483
4. Seifert L et al (2023) The classical pathway triggers pathogenic complement activation in membranous nephropathy. Nat Commun 14(1):473
5. Liu WJ et al (2017) Blockage of the lysosome-dependent autophagic pathway contributes to complement membrane attack complex-induced podocyte injury in idiopathic membranous nephropathy. Sci Rep 7(1):8643
6. Dong Z et al (2021) Inhibition of the Wnt/beta-catenin signaling pathway reduces autophagy levels in complement treated podocytes. Exp Ther Med 22(1):737
7. Yang Y et al (2022) Regulation of SIRT1 and Its Roles in Inflammation. Front Immunol 13:831168
8. Liu T et al (2022) Comprehensive bibliometric analysis of sirtuins: Focus on sirt1 and kidney disease. Front Pharmacol 13:966786
9. Jin Q et al (2024) Roles of Sirt1 and its modulators in diabetic microangiopathy: A review. Int J Biol Macromol 264(Pt 2):130761
10. Sun T et al (2015) Acetylation of Beclin 1 inhibits autophagosome maturation and promotes tumour growth. Nat Commun 6:7215
11. Xu Y, Wan W (2023) Acetylation in the regulation of autophagy. Autophagy 19(2):379–387
12. Cybulsky AV, Quigg RJ, Salant DJ (2005) Experimental membranous nephropathy redux. Am J Physiol Ren Physiol 289(4):F660–F671
13. Beck LH Jr., Salant DJ (2014) Membranous nephropathy: from models to man. J Clin Invest 124(6):2307–2314
14. Sinico RA et al (2016) Immunology of membranous nephropathy: from animal models to humans. Clin Exp Immunol 183(2):157–165

15. Borza DB (2016) Alternative Pathway Dysregulation and the Conundrum of Complement Activation by IgG4 Immune Complexes in Membranous Nephropathy. Front Immunol 7:157
16. Gao S, Cui Z, Zhao MH (2022) Complement C3a and C3a Receptor Activation Mediates Podocyte Injuries in the Mechanism of Primary Membranous Nephropathy. J Am Soc Nephrol 33(9):1742–1756
17. Zhang Q et al (2024) C3aR-initiated signaling is a critical mechanism of podocyte injury in membranous nephropathy. JCI Insight, 9(4)
18. Lee IH et al (2008) A role for the NAD-dependent deacetylase Sirt1 in the regulation of autophagy. Proc Natl Acad Sci U S A 105(9):3374–3379
19. Su PP et al (2022) Down-regulation of Risa improves podocyte injury by enhancing autophagy in diabetic nephropathy. Mil Med Res 9(1):23
20. Han X et al (2023) Placental Mesenchymal Stem Cells Alleviate Podocyte Injury in Diabetic Kidney Disease by Modulating Mitophagy via the SIRT1-PGC-1alpha-TFAM Pathway. Int J Mol Sci, 24(5)
21. Hariharan N et al (2010) Deacetylation of FoxO by Sirt1 Plays an Essential Role in Mediating Starvation-Induced Autophagy in Cardiac Myocytes. Circ Res 107(12):1470–1482
22. Kuno A, Horio Y (2016) *SIRT1: A Novel Target for the Treatment of Muscular Dystrophies.* Oxid Med Cell Longev, 2016: p. 6714686
23. Kim JY et al (2022) SIRT1 and Autophagy: Implications in Endocrine Disorders. Front Endocrinol (Lausanne) 13:930919
24. Yamamoto T et al (2016) Cardiac Sirt1 mediates the cardioprotective effect of caloric restriction by suppressing local complement system activation after ischemia-reperfusion. Am J Physiol Heart Circ Physiol 310(8):H1003–H1014
25. Zhong F et al (2019) Complement C3 activation regulates the production of tRNA-derived fragments Gly-tRFs and promotes alcohol-induced liver injury and steatosis. Cell Res 29(7):548–561
26. Moruno F, Perez-Jimenez E, Knecht E (2012) Regulation of autophagy by glucose in Mammalian cells. Cells 1(3):372–395
27. Gu X et al (2016) SIRT1-mediated FoxOs pathways protect against apoptosis by promoting autophagy in osteoblast-like MC3T3-E1 cells exposed to sodium fluoride. Oncotarget 7(40):65218–65230
28. Luchetti F et al (2022) Melatonin Attenuates Ischemic-like Cell Injury by Promoting Autophagosome Maturation via the Sirt1/FoxO1/Rab7 Axis in Hippocampal HT22 Cells and in Organotypic Cultures. Cells, 11(22)
29. Deng Z et al (2021) SIRT1 attenuates sepsis-induced acute kidney injury via Beclin1 deacetylation-mediated autophagy activation. Cell Death Dis 12(2):217
30. Sun Y et al (2023) SIRT1 Promotes Cisplatin Resistance in Bladder Cancer via Beclin1 Deacetylation-Mediated Autophagy. Cancers (Basel), 16(1)

31. Sun Y et al (2022) Inhibition of nuclear deacetylase Sirtuin-1 induces mitochondrial acetylation and calcium overload leading to cell death. Redox Biol 53:102334
32. Wang R et al (2019) ATP13A2 facilitates HDAC6 recruitment to lysosome to promote autophagosome-lysosome fusion. J Cell Biol 218(1):267–284
33. Zencheck WD, Xiao H, Weiss LM (2012) Lysine post-translational modifications and the cytoskeleton. Essays Biochem 52:135–145
34. Yoshida M et al (2017) Chemical and structural biology of protein lysine deacetylases. Proc Jpn Acad Ser B Phys Biol Sci 93(5):297–321
35. Iwahara N et al (2022) Activation of SIRT1 promotes membrane resealing via cortactin. Sci Rep 12(1):15328
36. Pacholec M et al (2010) SRT1720, SRT2183, SRT1460, and resveratrol are not direct activators of SIRT1. J Biol Chem 285(11):8340–8351
37. Wang YJ et al (2021) Modulating Sirtuin Biology and Nicotinamide Adenine Diphosphate Metabolism in Cardiovascular Disease-From Bench to Bedside. Front Physiol 12:755060
38. Hwang ES, Song SB (2017) Nicotinamide is an inhibitor of SIRT1 in vitro, but can be a stimulator in cells. Cell Mol Life Sci 74(18):3347–3362
39. Ogura Y, Kitada M, Koya D (2021) Sirtuins and Renal Oxidative Stress. Antioxid (Basel), 10(8)
40. Hasegawa K et al (2024) Ability of NAD and Sirt1 to epigenetically suppress albuminuria. Clin Exp Nephrol 28(7):599–607
41. Zhang M et al (2021) Quercetin 3,5,7,3',4'-pentamethyl ether from Kaempferia parviflora directly and effectively activates human SIRT1. Commun Biol 4(1):209
42. Rymarchyk S, Kang W, Cen Y (2021) Substrate-Dependent Sensitivity of SIRT1 to Nicotinamide Inhibition. Biomolecules, 11(2)
43. Kamble P et al (2015) Aspirin may influence cellular energy status. Eur J Pharmacol 749:12–19
44. Sui W et al (2015) Comparative proteomic analysis of membranous nephropathy biopsy tissues using quantitative proteomics. Exp Ther Med 9(3):805–810
45. Barkas G et al (2022) Targeted proteomic analysis dataset of archival core human kidney biopsies to investigate the biology of hypertensive nephropathy. Data Brief 40:107805

Figures

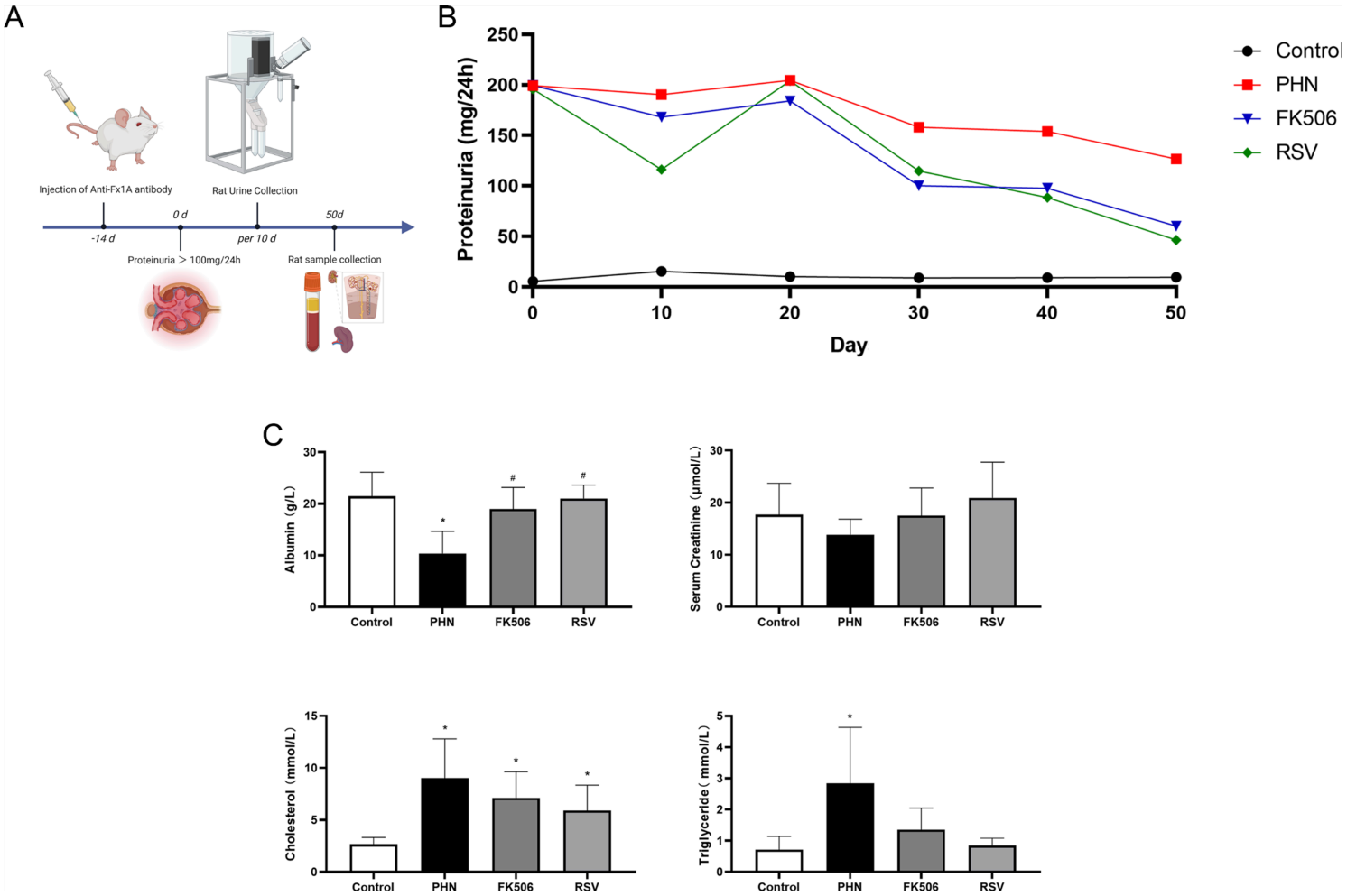


Figure 1

SIRT1 activation ameliorates proteinuria and renal function in PHN rats.

(A) Schematic diagram of the experimental timeline for the PHN rat model.

(B) 24-hour urinary protein excretion in rats from different groups.

(C) Blood biochemical parameters including serum albumin, cholesterol, triglycerides and serum creatinine were measured at day 50. *P < 0.05 vs. Control group; #P < 0.05 vs. PHN group.

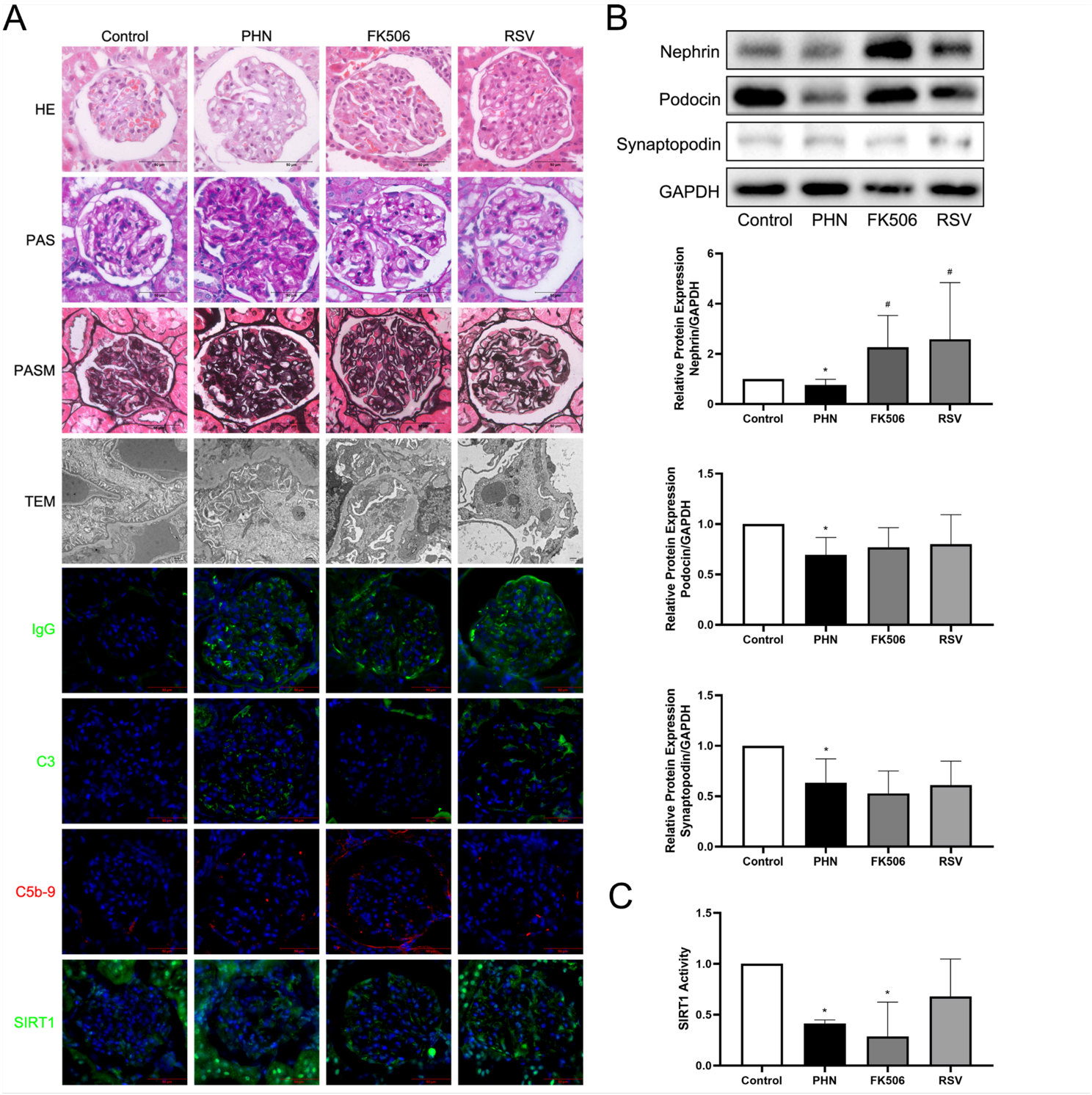


Figure 2

SIRT1 activation attenuates renal pathological damage and restores SIRT1 activity in PHN rats.

(A) Representative images of renal histology: H&E, PAS, and PASM staining showing glomerular basement membrane (GBM) thickening (black arrows). Electron microscopy (EM) images reveal foot process effacement (yellow arrows) and lysosome enlargement (red arrows). Immunofluorescence (IF) staining shows deposits of IgG, C3, C5b-9, and the expression of SIRT1 in glomeruli. 400× (light microscopy and IF), 15000× (EM).

(B) Western blot analysis of podocyte marker proteins (Nephrin, Podocin, Synaptopodin) in renal tissues. GAPDH served as a loading control. Densitometric quantification is shown. *P < 0.05 vs. Control group; #P < 0.05 vs. PHN group.

(C) SIRT1 enzymatic activity was measured in renal cortical tissues. *P < 0.05 vs. Control group.

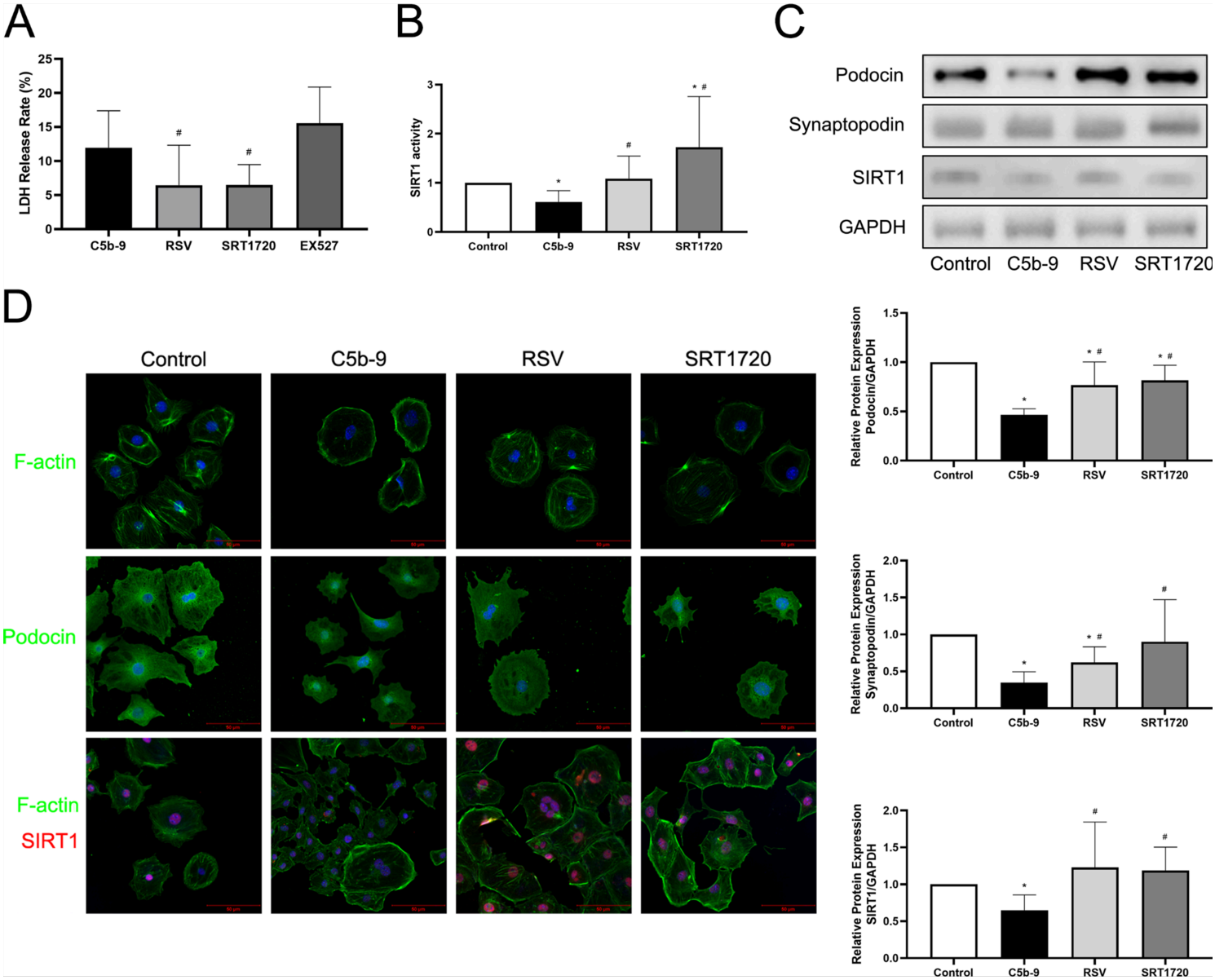


Figure 3

SIRT1 activation protects against complement-mediated injury in podocytes.

(A) LDH release assay assessing podocyte damage after ZAS challenge and SIRT1 agonist (RSV or SRT1720) pretreatment. #P < 0.05 vs. C5b-9 group.

(B) SIRT1 enzymatic activity in podocytes. *P < 0.05 vs. Control group; #P < 0.05 vs. C5b-9 group.

(C) Western blot analysis of podocyte markers (Podocin, Synaptopodin) and SIRT1 expression. GAPDH served as a loading control. Densitometric quantification is shown. *P < 0.05 vs. Control group; #P < 0.05 vs. C5b-9 group.

(D) Immunofluorescence staining of F-actin (Phalloidin, green), Podocin (green), and SIRT1 (red). Nuclei were counterstained with DAPI (blue). Scale bar: 50 μm.

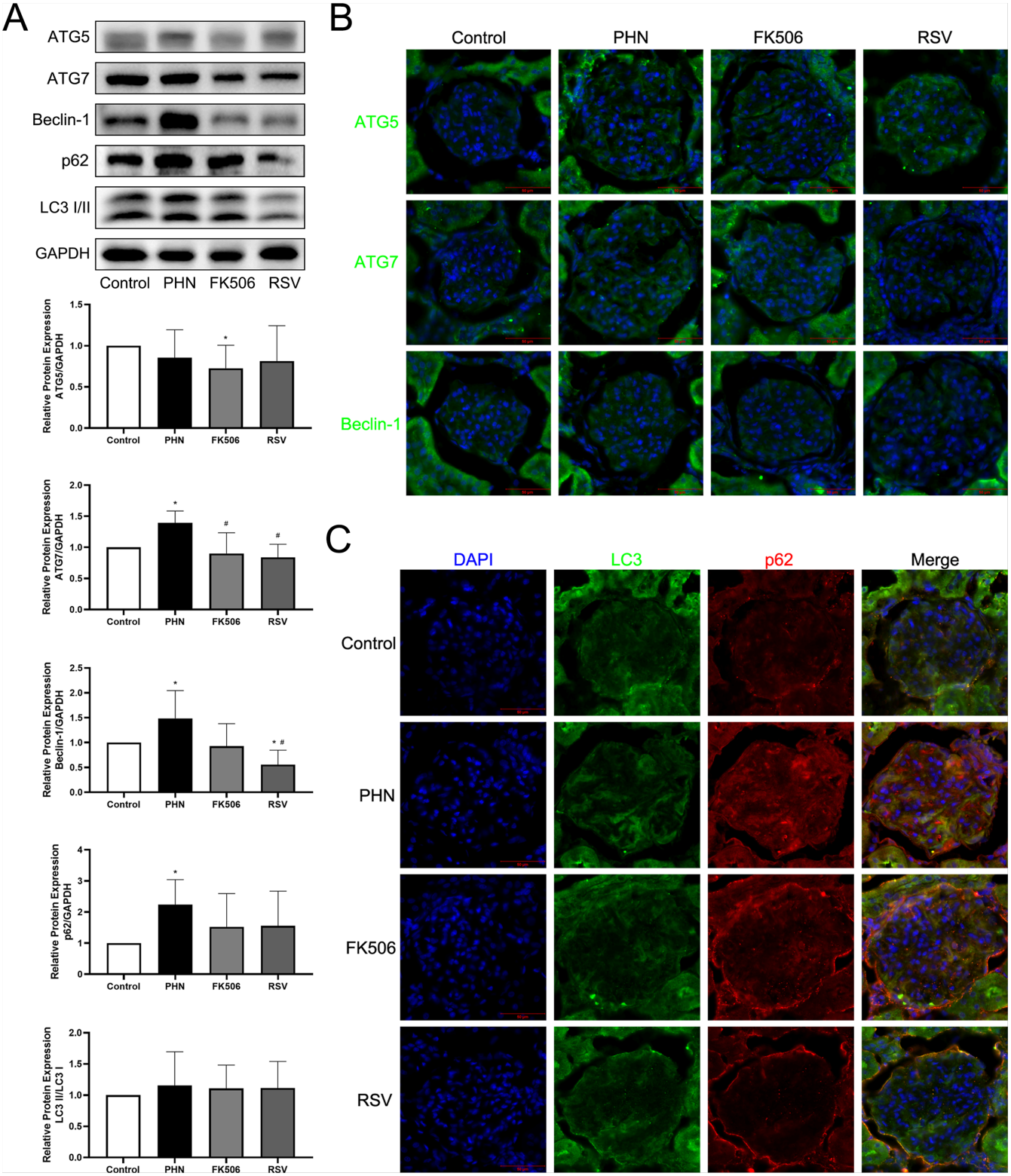


Figure 4

SIRT1 regulates autophagy in renal tissues of PHN rats.

(A) Western blot analysis of autophagy-related proteins (ATG5, ATG7, Beclin-1, p62, LC3) in renal cortical tissues. GAPDH served as a loading control. Densitometric quantification is shown. *P < 0.05 vs. Control group; #P < 0.05 vs. PHN group.

(B) Immunofluorescence staining of ATG5, ATG7, and Beclin-1 in glomeruli. 400×.

(C) Immunofluorescence staining and colocalization analysis of p62 (red) and LC3 (green) in renal tissues. Yellow in the merged images indicates colocalization. 400×.

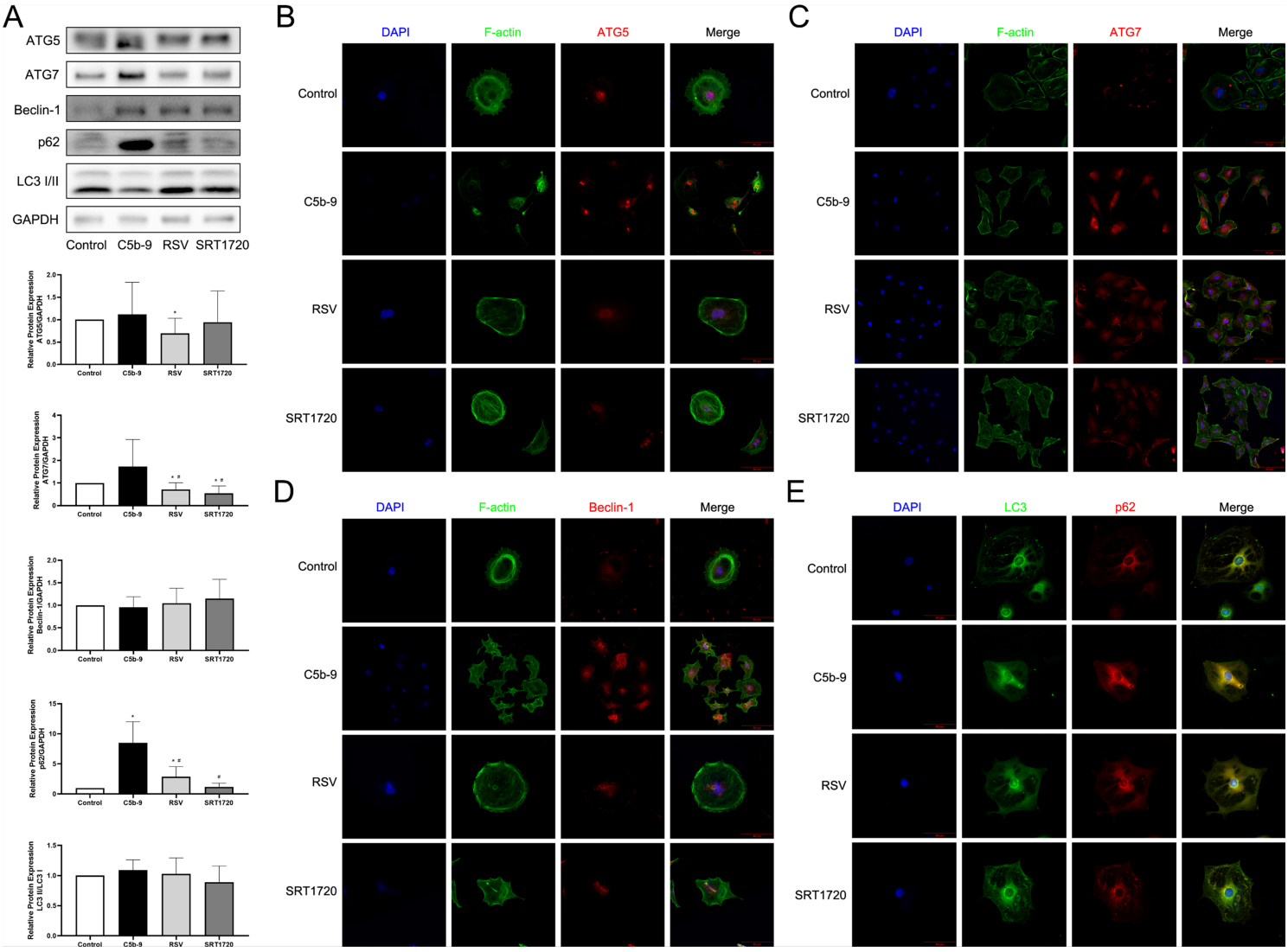


Figure 5

SIRT1 resolves blocked autophagic flux in injured podocytes.

(A) Western blot analysis of autophagy-related proteins (ATG5, ATG7, Beclin-1, p62, LC3) in podocytes. GAPDH served as a loading control. Densitometric quantification is shown. *P < 0.05 vs. Control group; #P < 0.05 vs. C5b-9 group.

(B-E) Immunofluorescence staining and colocalization analysis of (B) ATG5, (C) ATG7, (D) Beclin-1, (E) p62 (all in red) with LC3 (green). Nuclei were counterstained with DAPI (blue). Yellow in the merged images indicates colocalization. Scale bar: 50 μm.

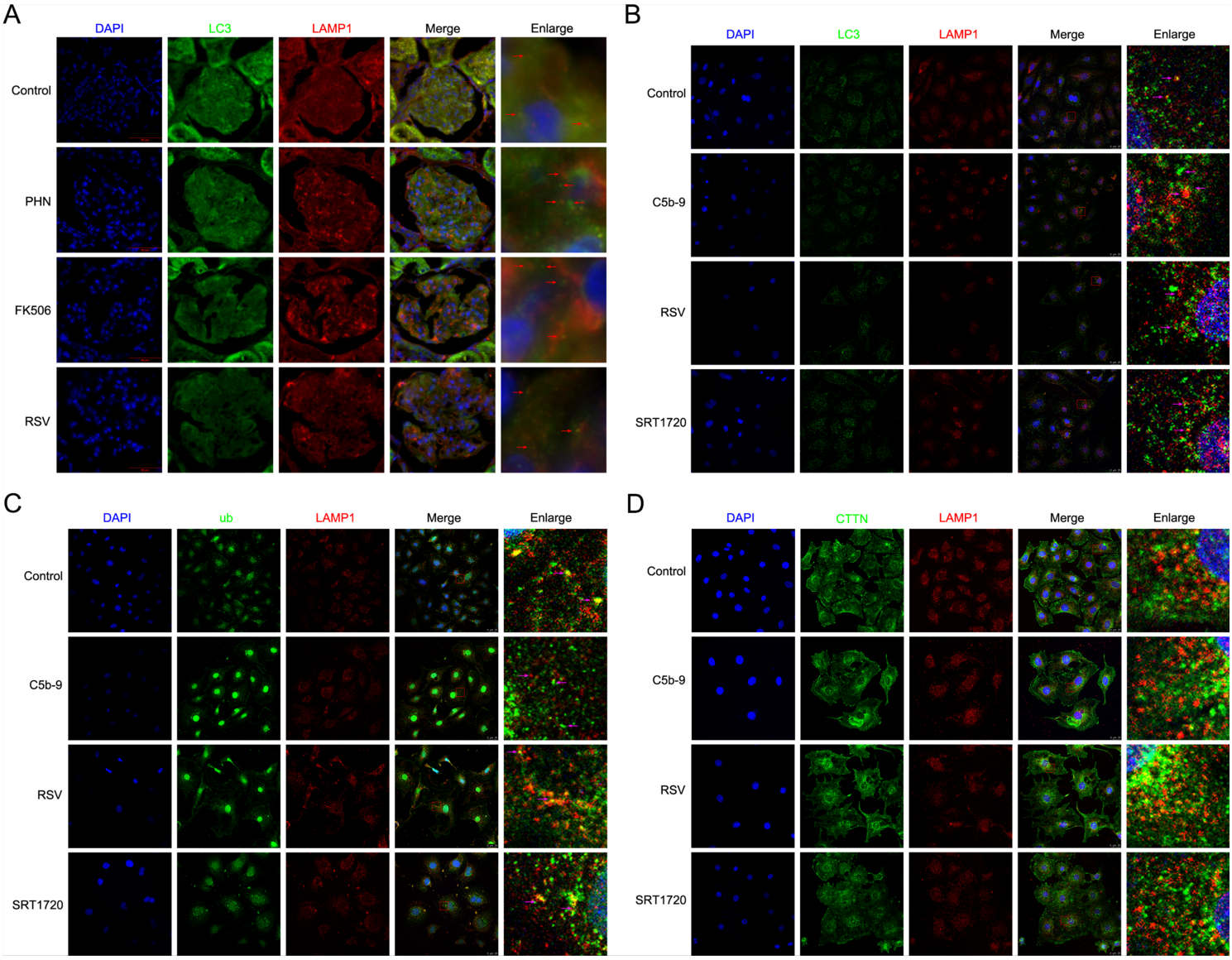


Figure 6

SIRT1 promotes autophagosome-lysosome fusion.

(A) Immunofluorescence colocalization analysis of LC3 (green) and the lysosomal marker LAMP1 (red) in glomeruli. Yellow indicates colocalization. 400×.

(B-D) Immunofluorescence colocalization analysis in podocytes: (B) Ubiquitin (Ub, green) and LAMP1 (red); (C) LC3 (green) and LAMP1 (red); (D) Cortactin (CTTN, green) and LAMP1 (red). Yellow indicates

colocalization. Scale bar: 50 μm.

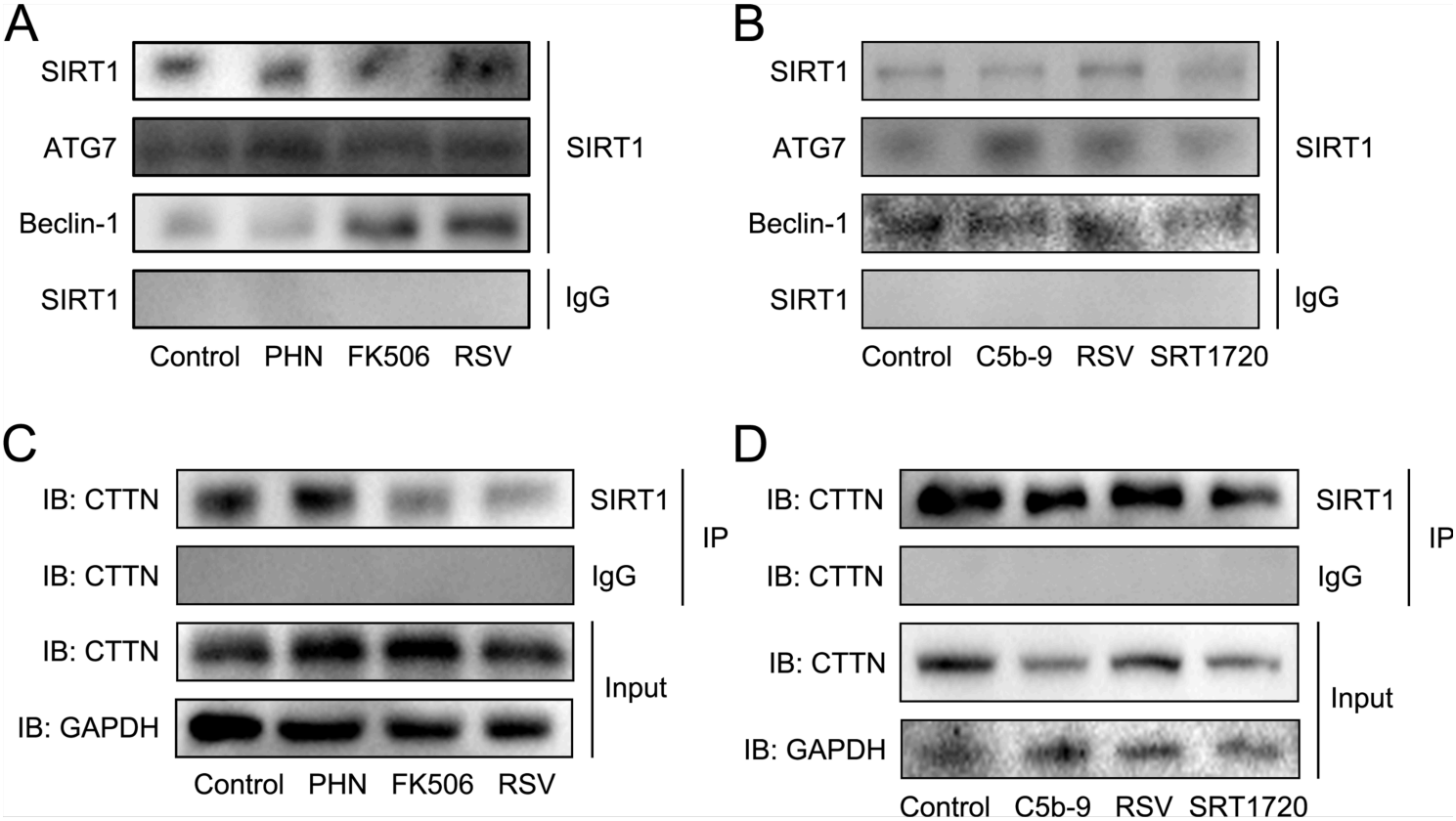


Figure 7

SIRT1 interacts with and deacetylates core autophagic proteins.

(A-B) Co-immunoprecipitation (Co-IP) assays demonstrating the interaction between SIRT1 and ATG7 or Beclin-1 in (A) renal tissues and (B) podocytes. IgG was used as a control.

(C-D) Co-IP assays demonstrating the interaction between SIRT1 and CTTN in (C) renal tissues and (D) podocytes. IgG was used as a control.

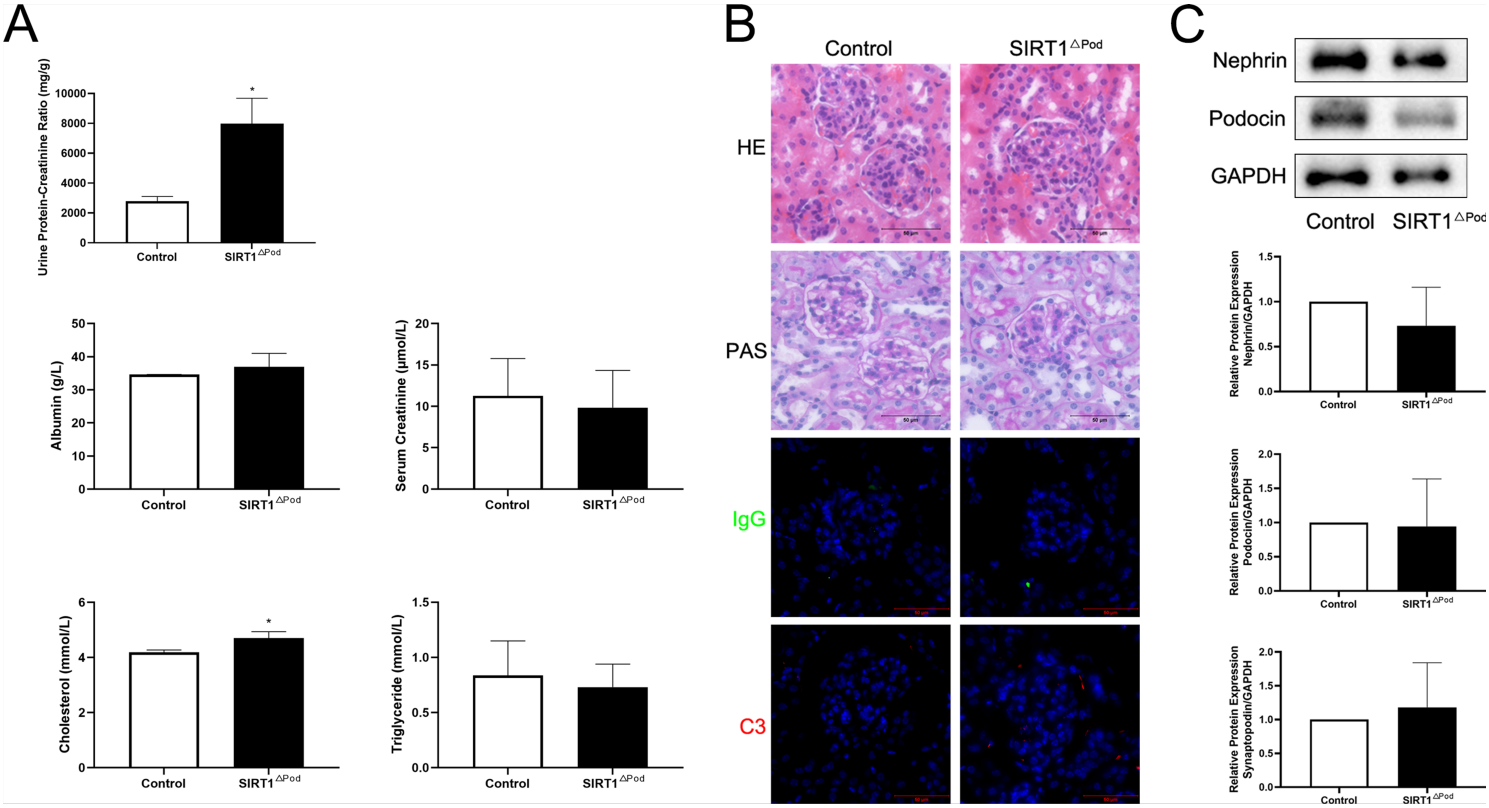


Figure 8

Podocyte-specific SIRT1 knockout leads to mild podocyte dysfunction in aged mice.

(A) Urinary albumin-to-creatinine ratio (UACR) and serum albumin, cholesterol, triglycerides and serum creatinine in SIRT1$^{\triangle Pod}$ mice and their littermate controls. *P < 0.05 vs. Control group.

(B) Renal histology (H&E and PAS staining) and immunofluorescence for IgG and C3 deposition. Scale bar: 50 μm.

(C) Western blot analysis of podocyte markers (Nephrin, Podocin) in renal tissues of SIRT1$^{\triangle Pod}$ mice and controls. GAPDH served as a loading control. Densitometric quantification is shown. *P < 0.05 vs. Control group.

Supplementary Files

This is a list of supplementary files associated with this preprint. Click to download.

- supplementarymaterials.docx
- SupplementaryInformation.pdf